30 June 1978, Volume 200, Number 4349 SCIENCE

# EXAFS: New Horizons in Structure Determinations

P. Eisenberger and B. M. Kincaid

*Summary.* Although the phenomena of extended x-ray absorption fine structure (EXAFS) were observed as early as the 1930's, EXAFS has only recently, with the utilization of synchrotron radiation, been transformed into a powerful structural technique. The theory and experimental practice of the technique are described and illustrated with data on germanium. Applications to systems as diverse as hemoglobin, polymer-bound catalysts, ions in solution, amorphous solids, and adsorbate atoms on surfaces are reviewed. With the recent approval of funding for new, more powerful dedicated synchrotron sources, the future holds the possibility of a virtual revolution in structure determinations.

As early as the 1930's, it had been observed that the absorption cross section in the x-ray regime had a complex structure as a function of energy extending as far as 1000 electron volts above an absorption threshold (*1*). These measurements were made by using a low-power conventional x-ray tube, a dispersive Bragg spectrometer, and film as a detector. After some correct and incorrect speculation concerning the origin of this extended x-ray absorption fine structure (EXAFS), the field remained essentially dormant through the 1950's. In the late 1960's the measurements were revived (*2*), this time using modern counting and automation techniques. The previous interpretation (*3–5*) of the structure as arising from the backscattering of the ejected photoelectron from the atoms near the absorbing site was strongly supported. The idea that this phenomenon might be used as local structural probe was born. However, even with the experimental advances the measurements were difficult and time-consuming because of the low power of the x-ray source. This limited the application of the technique to highly concentrated systems and also inhibited the systematic study of the phenomenon that was necessary to turn the semiquantitative interpretations into quantitative evaluations.

In 1972 the bremsstrahlung radiation produced by a conventional x-ray tube was replaced in the experiments by synchrotron radiation produced by high-energy storage rings (*6–8*). The increase in flux of approximately $10^5$ to $10^6$ provided by the Stanford storage ring SPEAR signaled the beginning of a virtual revolution in the quantitative understanding of EXAFS (*9–12*). In the last 3 years EXAFS has been successfully applied to determining the structural arrangement of as few as $10^{13}$ atoms on a single-crystal surface and of complex, dilute, and disordered systems that were previously inaccessible. These studies have spanned the scientific disciplines of biology, chemistry, and solid-state and surface science. In this article we summarize the current quantitative understanding of EXAFS and describe how the measurements are made. We then give some representative examples of the successful applications of this technique to the study of structural problems in these fields.

P. Eisenberger is head of the Electromagnetic Phenomena Research Department and B. M. Kincaid is a Member of the Technical Staff at Bell Laboratories, Murray Hill, New Jersey 07974.

## Theory, Experiment, and Analysis

X-rays are absorbed by matter primarily through the photoelectric effect. Figure 1a shows that photoelectric absorption occurs when a bound electron, in this case in the $K$ shell, is excited to a continuum state by an incident photon of energy $E = \hbar\omega$, where $\hbar$ is Planck's constant divided by $2\pi$ and $\omega$ is the frequency of the photon. The final electron has the energy $\hbar\omega - E_K$, where $E_K$ is the $K$ shell binding energy. For photon energies less than $E_K$ this excitation is not possible, so that if one makes a transmission measurement with x-rays, as illustrated in Fig. 1b, and measures the absorption coefficient $\mu$ as a function of photon energy, a sharp rise or edge is observed at the $K$ shell threshold energy. Since each element has its own unique $E_K$, it is possible to study one kind of atom in the presence of many others by tuning the x-ray energy to the proper absorption edge.

Figure 2 is a diagram of an experimental setup at the SPEAR storage ring designed to use synchrotron radiation to measure x-ray absorption. It consists of a condensing mirror, a parallel crystal monochromator, and a pair of ion chambers for measuring the intensity of the incident and transmitted radiation, $I_0$ and $I$, as shown in Fig. 1b. The parallel crystal monochromator selects a narrow band of radiation from the continuous spectrum produced by the stored electron beam in the SPEAR ring. By changing the Bragg angle of reflection in the monochromator, the output photon energy may be varied over a wide range, allowing one to study the $K$ edges of elements from potassium to copper in the periodic table—that is, from a photon energy of about 3 to about 9 kiloelectron volts. Other instruments similar to this


0036-8075/78/0630-1441$01.75/0 

one cover the larger energy range necessary to reach the $K$ edges of elements up to iodine, approximately 35 keV, and the $L$ edges of elements through the end of the periodic table. Other methods of measuring EXAFS have been developed, including the fluorescence method, in which the fluorescence photons of the atom of interest are measured as an indication of absorption rather than the transmitted flux. This removes the background absorption of the other constituents in dilute systems. In another variation one observes the Auger electrons produced when atoms that have absorbed a photon relax. This has proved very successful in surface studies in a vacuum.

In simple monatomic systems such as krypton gas, the absorption coefficient decreases monotonically above the $K$ edge, consistent with the theory of photoabsorption, as can be seen in Fig. 3. For a diatomic gas such as bromine ($Br_2$), however, sinusoidal oscillations are observed. These are the EXAFS oscillations, which are due to a final-state interference effect involving scattering of the outgoing photoelectron from the neighboring atoms, as shown schematically in Fig. 4, a and b. In Fig. 4a the absorption of a photon by a germanium atom in a crystal of germanium is shown. For simplicity, only the four nearest neighbors are shown. The outgoing electron is shown as a spherical wave, whose wavelength $\lambda_e = 2\pi/k$ depends on the energy of the electron, $\hbar\omega - E_0$, according to the formula

$$k = \left(\frac{2m(\hbar\omega - E_0)}{\hbar^2}\right)^{1/2} \qquad (1)$$

where $E_0$ is the threshold energy and $m$ is the mass of the electron. The scattered wave from the near neighbors overlaps the absorption site, the $K$ shell, and can interfere constructively or destructively, depending on the total phase shift experienced by the electron. This phase shift depends, in turn, on the distance between atoms, the wavelength of the electron and hence the incident photon energy, and the propagation of the electron between the absorbing site and the scattering atom. Figure 4b shows the change in the wave pattern that occurs when a lower-energy photon is absorbed. The electron wavelength is increased, changing the total phase shift and hence the amount of interference. Much theoretical work has gone into quantifying this simple picture of EXAFS (*10–12*). The generally accepted formula for EXAFS in a system with many interatomic distances is

$$\chi(k) = \sum_j \frac{-N_j|f_j(k, \pi)|}{kR_j^2} \times e^{-2\sigma_j^2k^2}e^{-2\lambda R_j} \sin [2kR_j + \delta_j(k)] \qquad (2)$$

Here $\chi(k)$ is the fractional modulation of the absorption coefficient due to EXAFS interference; that is

$$\chi(k) = \frac{\Delta\mu}{\mu_0}$$

where $\mu_0$ is the absorption coefficient without EXAFS—that is, for an isolated atom with no neighbors; $N_j$ is the number of scattering atoms at distance $R_j$; $|f_j(k, \pi)|$ is the electron scattering amplitude in the backward direction for the $j$th atom; $e^{-2\sigma_j^2k^2}$ is a Debye-Waller factor due to thermal vibrations or static disorder with root-mean-square fluctuation $\sigma_j$; $e^{-2\lambda R_j}$ is a term accounting for the loss of photoelectrons to inelastic scattering processes, $\lambda$ being the inverse mean free path; and $\sin [2kR_j + \delta_j(k)]$ is the sinusoidal interference term, $\delta_j(k)$ being the phase shift function.

Obviously EXAFS spectra contain a large amount of information about the material being studied. The problem in analyzing EXAFS data is to "peel the onion" of Eq. 2 and extract the values of $R_j$, $\delta_j(k)$, $N_j$, and so on. The steps in this process are outlined in Figs. 5, 6, 7, 8a, and 8b. Figure 5 shows the absorption spectrum of crystalline germanium at 100 K. The structure of germanium is well known; here it serves only as an example of how the analysis works. The sharp rise at about 11 keV is the $K$ edge, and the random-looking modulations above the edge are due to the EXAFS sine waves from several shells of neighboring atoms adding together. The first step in the analysis of EXAFS data is extracting $\chi(k)$ from the absorption coeffi-

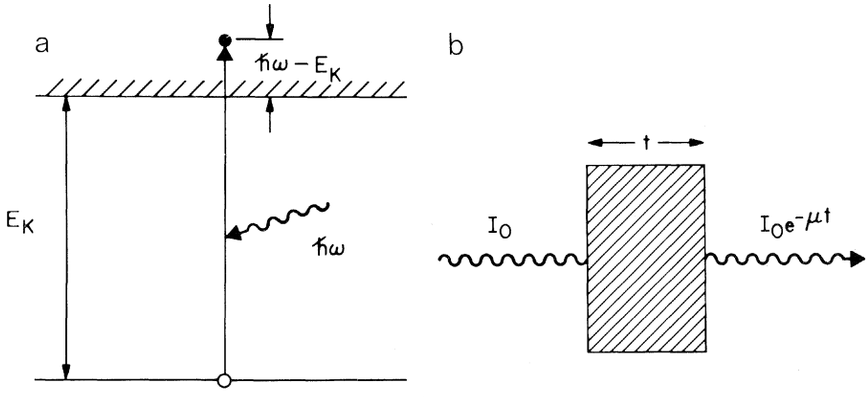


Fig. 1. (a) Schematic representation of the transition from a core state with binding energy $E_K$ to a state with a hole left behind and a photoelectron with energy $\hbar\omega - E_k$. (b) Schematic depiction of the attenuation of a beam of photons as they pass through a medium with absorption coefficient $\mu$ and thickness $t$.

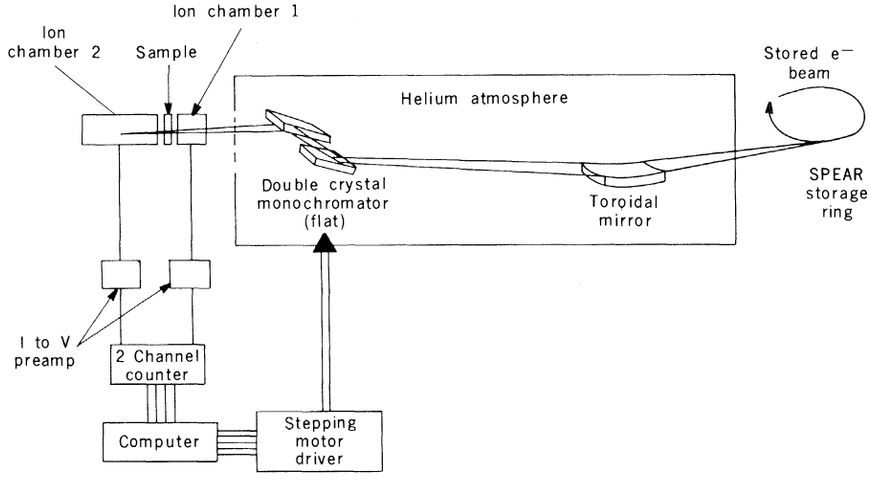


Fig. 2. The radiation emitted by the circulating electrons is collected by a toroidal mirror and monochromatized by a Bragg crystal spectrometer. The incident intensity is measured by ion chamber 1 and the transmitted beam by ion chamber 2. The energy of the beam is changed by changing the angle that the monochromator crystal makes with incident beam. A typical flux is $10^{10}$ photons per second per electron volt in an area of 3 square millimeters.

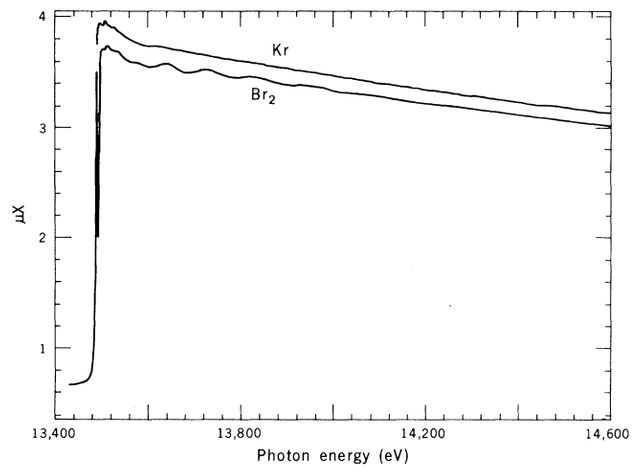


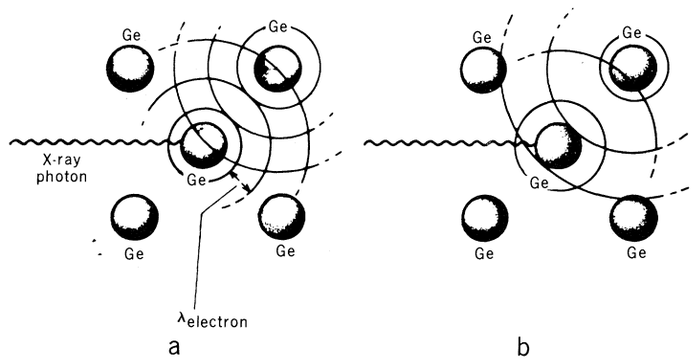


Fig. 3 (left). Energy-dependent absorption of Kr gas (no EXAFS) compared with the spectrum of diatomic $Br_2$, which has EXAFS superimposed. On the ordinate $X$ is the thickness of the samples. Fig. 4 (right). The sinusoidal EXAFS pattern can be understood as the changing interference pattern between the outgoing wave and the scattered wave at the absorbing site with the changing photoelectron wavelength (energy). In (a) the wavelength is such that the interference is constructive, while in (b), at a different electron wavelength, the interference is destructive.

cient data, $\mu(E)$. Since $\mu_0(E)$ is in general unknown, we use just the smooth part of $\mu(E)$ as $\mu_0$ and the remaining wiggly part as $\Delta\mu$. Furthermore, since the sharp rise in $\mu(E)$ at the edge does not necessarily correspond to the threshold energy for EXAFS (nor to $E_K$, for that matter), there is some ambiguity concerning the choice of $E_0$, and hence the definition of $k$ (Eq. 1) and therefore the phase shift $\delta_j(k)$ are also ambiguous. This problem is resolved by making $E_0$ a variable parameter in later stages of the analysis, as will be discussed later.

Figure 6 shows the EXAFS modulation after converting from $\hbar\omega$ to $k$ and removing the smooth $\mu_0$ background. In addition, the resulting $\chi(k)$ curve has been mutliplied by $k^3$. This $k^3$ factor cancels one power of $k$ in Eq. 2 and in addition roughly compensates for the $1/k^2$ behavior of $|f_j(k,\pi)|$ at large values of $k$. This has the effect of weighting the EXAFS oscillations more or less uniformly over a range of $k$ starting at about $k = 4$ Å$^{-1}$, corresponding to a photoelectron energy of about 60 eV above the edge. This weighting ensures that chemical effects on the EXAFS information will be minimized, since their effect on electrons with a kinetic energy greater than 60 eV will be small. At this stage of the analysis it is possible to try to use curve-fitting techniques to extract information from the data. In general, however, this is a difficult task because of the large number of parameters to be varied and the correlations among the parameters, which are difficult to avoid.

Therefore, the next step in the analysis is a Fourier transform. This isolates the contributions of the different shells of neighbors and allows us to use filtering techniques to study each shell separately. Figure 7 shows the magnitude of the Fourier transform of the curve in Fig. 6. The large peak is the contribution from the first shell of neighbors in germanium—four atoms at a distance of 2.45 Å. The Fourier transform peaks at a lower distance because of the effect of the phase shift $\delta_j(k)$. Several other smaller peaks that are visible above the noise correspond to more distant neighbors, but the signal-to-noise ratio is not as good as for the first shell. The dashed line in Fig. 7 is a smooth filter window function that is applied to the Fourier transform of $\chi(k)$ to isolate the EXAFS from the first shell. The inverse transform is then done, producing the solid curve in Fig. 8a. Notice that all the higher-frequency variations have been filtered out, and that we are left with a well-behaved sine wave. The Fourier transform also has the ability to decompose the sine wave into a unique amplitude and phase function. The amplitude is the dashed line in Fig. 8a, and the phase function is shown in Fig. 8b.

Hence, we are able to extract the amplitude and phase of a single term in Eq. 2. The phase function contains a term $2kR_j$ and a term $\delta_j(k)$. If $\delta_j(k)$ were known, we could determine the distance $R_j$ very accurately by simple subtraction. Of course, the value of $R_j$ is known for germanium, so we can subtract $2kR_j$ from the empirically determined phase shift and get an empirical $\delta_j(k)$. Furthermore, if $\delta_j(k)$ is truly independent of chemical environment, as was suggested earlier, we can use this empirical $\delta_j(k)$ to determine the distance $R_j'$ in a system with an unknown structure containing pairs of germanium atoms. In this comparison, $E_0$ must be a variable parameter adjusted to achieve the best fit of the phase shift of the model system to that of the unknown system. This is the idea of chemical transferability of phase shifts (*9*), a concept that has been successfully applied to a large class of materials and has been used to determine distances to 0.01 Å or better. Notice that this procedure does not separate $\delta_j(k)$ into parts corresponding to the absorbing atom and the scattering atom. All we can get from EXAFS measurements is the sum of the two, the total $\delta_j(k)$ for a pair of atoms, in this case two germanium atoms. Very accurate theoretical work has been done to calculate $\eta(k)$, the phase shift of the absorbing atom, and $\arg[f_j(k,\pi)]$, the phase shift of the scattering atom, but a comparison with experiment checks only the total, $\delta_j(k)$ (*12*).

The amplitude function produced by the Fourier transform filtering analysis has information about the number of nearest neighbors, the kind of atoms involved, the amount of disorder, and the electron mean free path. In systems where the first shell of neighbors has two or more kinds of atoms at slightly different distances, and where the Fourier transform technique cannot resolve the different species, curve fitting of the filtered data (Fig. 8a), which includes fitting the amplitude function, has been used successfully to determine distances, again to about 0.01 Å (*13*). The curve-fitting problem is still complicated by the number of parameters to be determined, but at least the Fourier transform filtering method reduces the number somewhat, as well as reducing the noise and the contributions from other unwanted shells.

## Biology

The structural problems confronting the biologist are truly immense. However, many of the large interesting biological molecules have a unique heavy atom that plays a significant role in the functioning of the molecule. These two features make EXAFS a very attractive technique for studying the structure-function relationship in large metalloproteins (*14*). Besides being very complex structurally many of these systems cannot be crystallized and therefore x-ray diffraction studies are difficult or impossible; even in the systems that can be crystallized, there is always the concern that the crystallized form may not be identical to the biologically active form. Being sensitive to short-range order in atomic arrangements rather than long-range crystalline order, EXAFS can be used equally well for systems in solution and in crystalline form. Furthermore, even if x-ray diffraction can be done, one must determine the positions of all the atoms. The strength of the EXAFS technique is that it can focus on one region in a large molecule (that is, around the heavy atom). If that region is where the structure-function relationship is centered, the structural information obtained will be more accurate than that given by an x-ray diffraction study of the whole structure. Two of the many applications of EXAFS to metalloproteins that illustrate this very clearly are the studies of rubredoxin and hemoglobin.

In 1972 Jensen and co-workers (*15, 16*) performed an x-ray diffraction study of rubredoxin in which they determined the structure of the iron-sulfur protein of molecular weight 8000. A significant feature of their structural determination was that the iron atom was surrounded by four sulfurs with an average bond length of 2.24 Å, but with one bond an anomalously short 2.05 Å. It was argued that this short bond was appreciably strained by the protein and thus could be involved in a mechanism by which the protein affected the redox potential and thus the electron transfer function of the molecule. Several EXAFS studies were performed on oxidized and reduced rubredoxin (*17–20*), and several iron-sulfur model systems of lower molecular weights. Initially transmission techniques were used (*17–19*), but eventually greater accuracy was obtained with fluorescence techniques (*20*). The initial transmission studies (*17, 18*) ruled out a spread in distances as large as that proposed by Jensen and co-workers, since no beat indicating such a spread was observed in the EXAFS pattern. Studies of the model systems, which had a small spread in the iron-sulfur distances, showed that the average distance could be determined to ± 0.015 Å and the absolute value of the spread in distances to about ± 0.05 Å. Fluorescence EXAFS studies of oxidized and reduced rubredoxin in the crystalline and solution forms showed a 0.06-Å change on reduction (2.26 to 2.32 Å). In addition, by using various analytical procedures (*20*), it was shown that the spread in the iron-sulfur distances in oxidized rubredoxin was 0.04 ± 0.05 Å. The spread due to thermal vibrations is approximately 0.05 Å, so there is no indication that there is an anomalously short iron-sulfur bond that is energetically (functionally) significant. Subsequent x-ray diffraction results (*21*) considerably reduced the spread in iron-sulfur distances from 0.25 to 0.10 Å. Thus, within the experimental uncertainties, the two techniques now agree.

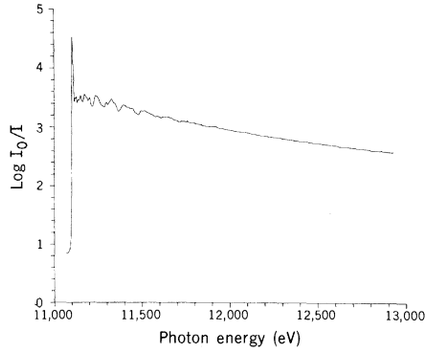


Fig. 5. Absorption spectrum of powdered crystalline germanium. The complex oscillatory structure is due to the presence of many different sinusoidal frequencies (distances), each corresponding to a different shell of neighboring germanium atoms.

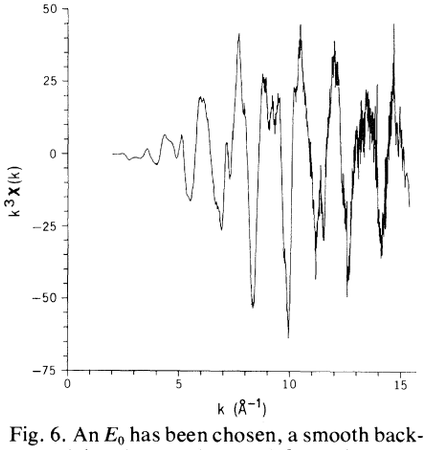


Fig. 6. An $E_0$ has been chosen, a smooth background has been subtracted from the spectrum in Fig. 5, and the result, after division by the smooth background, has been multiplied by $k^3$ to generate $k^3\chi(k)$ as a function of $k$, which is given by Eq. 1.

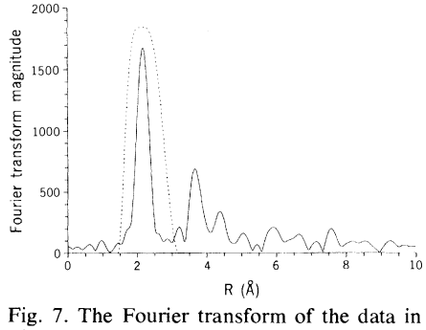


Fig. 7. The Fourier transform of the data in Fig. 6 is shown together with the filter function (dashed line) used to isolate the contribution of the first shell. Other, more distant shells are also visible.

Hemoglobin has been extensively studied by many techniques, including x-ray diffraction (*22*). It is a protein with four iron atoms per molecule, with each iron being bonded to the planar porphyrin structure as well as an axial histidine nitrogen and a sixth ligand, oxygen, in the oxy form. Those studies have attempted to identify the structural cause of the switch in hemoglobin from the low- to the high-oxygen-affinity state as well as to characterize the structural differences between the two states. The affinity change is responsible for the long-recognized cooperativity of oxygen binding that is exhibited by hemoglobin. Since the four neighboring iron subunits in hemoglobin are separated by 35 Å, it is difficult to imagine how the binding of oxygen at one site could affect the oxygen affinity of an iron atom at a neighboring site. Initial models for this effect were formulated on the basis of the pioneering x-ray diffraction work of Perutz (*23*). That work identified a 0.75-Å motion of the iron atom into the porphyrin plane on oxygen binding. This large initial displacement of the iron atom from the porphyrin plane was thought to explain the low initial affinity for oxygen (that is, it was hard for the oxygen to get to the iron atom). The large motion on oxygen binding was thought to act like a plunger which could change the structure at a neighboring iron site and thus switch it from low to high affinity. Initial fluorescence EXAFS studies (*24*) of hemoglobin were performed in both normal hemoglobin and Kempsey hemoglobin, a mutant form that is always in the high-affinity state. They showed that both forms had the same average iron-nitrogen in-plane distance within 0.01 Å. Thus, here again, as in rubredoxin, speculation that a localized strain near a special atom was responsible for the function of the protein proved incorrect.

A subsequent study of hemoglobin (*25*) and smaller iron porphyrin model

systems evaluated the average distance between the iron atom and the porphyrin ring nitrogens. This required special methods of data analysis in which the nearest-neighbor shell was first isolated and the contribution of the axial ligands was then removed. The results were 1.98 Å for oxyhemoglobin and 2.05 Å for normal and Kempsey deoxyhemoglobin. The results for the lower-molecular-weight model systems were in agreement with the x-ray diffraction results. In particular, the results for the "picket fence" porphyrins, which also reversibly bind oxygen, were in agreement with the x-ray diffraction results and showed the same distances as in hemoglobin. A 0.75-Å motion of the iron atom would have required a 0.14-Å change in the distance between an iron atom and a porphyrin nitrogen if the porphyrin ring itself did not change. The smallness of the observed iron–porphyrin nitrogen distance in deoxyhemoglobin may be partially attributable to the fact that the extra electron bound in the $Fe^{2+}$ state does not, as originally thought (*23*), go with the iron atom, but is distributed around the resonant porphyrin structure and thus does not significantly increase the size of the iron atom. Furthermore, studies of other high-spin $Fe^{2+}$ porphyrin systems show that the porphyrin ring is not rigid but actually changes in size and buckles in response to the strain of a change in radius of the central metal ion (*26*). The 0.07-Å observed change in iron porphyrin together with the data from the model systems enables one to place a limit of $0.2^{+0.3}_{-0.2}$ Å on the iron displacement from the porphyrin nitrogens on oxygen binding. Thus, as a result of EXAFS studies it is now suggested that the distortion associated with oxygen removal is not a single large iron displacement, but instead also involves a significant distortion of the porphyrin ring itself. Further studies on the more distant shells are needed to evaluate this distortion in detail.

The hemoglobin and rubredoxin studies are just two examples of a large body of research on large biological molecules. Another example is a very ambitious study of the nitrogen fixation enzyme, nitrogenase. One of the proteins in nitrogenase contains both iron and molybdenum, and it has now been determined that the environment of the molybdenum atom is probably an iron-sulfur cluster (*27*). Investigations of hemocyanin and cytochrome P-450, in particular for metal-metal interactions and calcium-binding and -containing proteins, have also been begun. There has been an interesting preliminary study of the binding of the potential anticancer drugs *cis*- and *trans*-$Pt(amine)_2Cl_2$ to DNA (*28*). The nature of the bonding has been determined, although attempts to distinguish between effective and ineffective drugs have been unsuccessful to date.

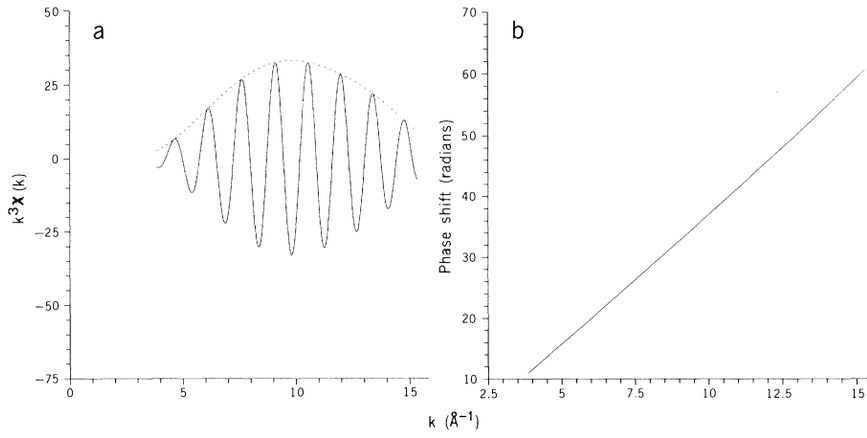


Fig. 8. The filtered version of Fig. 7 has been retransformed back to $k$ space with (a) the amplitude function (dashed line) and (b) the phase having been obtained separately by using the complex transform.

## Chemistry

Many of the structural questions of importance in chemistry involve systems that cannot be crystallized, and therefore structural determinations by non-EXAFS techniques are very difficult. Heterogeneous catalysts, supported catalysts, solutions, and chemically unstable metal clusters are some examples. Here again, it is frequently the case that a specific heavy atom can be identified with the function of the system and thus it can be readily studied by the EXAFS technique.

Heterogeneous catalysts have been most extensively studied (*13, 29–31*), both because of their potential technological importance and because of the difficulty of obtaining structural information by other means. A representative study was that of Wilkinson's catalyst (*13*), chlorotris(triphenylphosphine)rhodium[$(Ph_3P)_3RhCl$], which has been suggested as a hydrogenation catalyst, with polystyrene cross-linked with divinylbenzene as a supporting medium. The structure of the free catalyst has been determined by x-ray diffraction (*32*), but any attempt to determine the polymer-bound structure would be severely complicated by the large scattering from the supporting medium and the lack of crystallinity. Chemical studies had shown that on binding to a polymer with a low degree of cross-linking, two phosphorus atoms were released and there was a significant reduction in the catalytic activity. EXAFS studies of the rhodium atom were performed with both the free catalyst and the catalyst bound to a 2 percent cross-linked polymer. Since the nearest neighbors of rhodium in the free catalyst are one chlorine atom, two phosphorus atoms at one bond distance, and another phosphorus atom (opposite the chlorine) at a shorter distance, it would not be adequate to determine just the average nearest-neighbor distance. Therefore, in this case, the observed EXAFS spectrum, after Fourier transform filtering, was fitted by a model with three types of bonds, using the Rh-P and Rh-Cl scattering amplitudes and phase shifts from model systems and theoretical calculations.

This left nine free parameters, three coordination numbers, three bond distances, and three Debye-Waller factors to be determined by the fitting procedure. The results for the free catalyst agreed with the x-ray results in both coordination numbers and bond distances. The bond distances in angstroms, determined by EXAFS (and x-ray diffraction) were: Rh-Cl, 2.35 (2.38); $Rh\text{-}P_1$, 2.23 (2.21); and $Rh\text{-}P_2$, 2.35 (2.33). The EXAFS pattern for the polymer-bound catalyst was dramatically different and showed that the ratio of phosphorus to chlorine nearest neighbors had changed from 3:1 to 2:2. More detailed analysis showed a loss of the two longer phosphorus bonds (in agreement with chemical observations of the loss of two phosphorus bonds per bound molecule), which were replaced by a shorter Rh-P bond of length 2.16 Å. The two chlorine atoms were found to have bond distances of 2.33 Å and the remaining phosphorus was unchanged at 2.23 Å. More importantly, the presence of two chlorine atoms in the Rh(I) system clearly indicated that dimerization had oc-

curred and that the chlorine atoms bridge two rhodium atoms, which are probably in turn attached to the polymer by the short Rh-P bond. This dimerization would explain the observed reduction in catalytic activity. A subsequent study of the bromine form of Wilkinson's catalyst (*30*), in which the EXAFS structure of both rhodium and bromine was measured as a function of the amount of cross-linking, showed that by 20 percent cross-linking the structure was back to the high-activity monomeric form. These findings suggest that if there is a trade-off of catalytic activity as a function of cross-linking between a reduction in dimer formation and a decrease in free volume, then there is probably some optimum degree of cross-linking between 2 and 20 percent.

The initial application of EXAFS to solution chemistry was on a simple dilute solution of $CuBr_2$ in water (*33*). The distances from the $Cu^{2+}$ and $Br^-$ ions to their respective first hydration spheres were determined. In the 0.01 molar concentration region in which EXAFS measurements can be made, x-ray scattering experiments would be virtually impossible because of the large scattering background of the solvent.

The distance to the first hydration sphere in a dilute solution is only a small part of the information obtained by this technique. Studies have already been performed in which the hydration, including hydration number, was studied as a function of the concentration of solute (*34*). At intermediate concentrations more distant hydration spheres were observed (*35*), and at high concentrations cluster molecules formed (*34*). A surprising feature of these studies was the relatively low concentration at which cluster molecules formed that were similar in structure to the solid hydrated salt.

The study (*36*) of the chemically unstable one electron metal-metal bonded cobalt dimer $[(C_5H_5)CoP(C_6H_5)_2]_2^+$, which has a one-electron metal-metal bond, is a fine example of the ability of EXAFS to provide structural information that would otherwise be unattainable. In addition to determining the structure of the Co-Co dimer, this study provided the first opportunity to determine the effect of oxidation in a metal cluster when the electron removed was from a metal-metal bonding orbital. Previously, such systems could not be studied because the chemical instability made crystal growth impossible. The EXAFS spectrum before and after oxidation showed that the mean squared relative displacement of the metal-metal bond had increased by a factor of 3 after oxidation. A simple model indicated that the force constant had decreased by a factor of 3 on oxidation. Studies of the bond lengths, however, revealed only a 0.08-Å increase, which strongly suggested the presence of significant steric hindrances. The chemically stable systems previously studied had all shown a stiffening and a decrease in bond length on oxidation because in those systems antibonding electrons were removed.

## Solids and Surfaces

Structural characterizations of ordered solids can be obtained by x-ray, neutron, or electron diffraction. Ordered surface layers can be studied by low-energy electron diffraction (LEED), but with great interpretational difficulties. With alloys, amorphous solids, glasses, impurities on solids, and adsorbates on surfaces, however, only very simple systems can be characterized, and even then with extreme difficulty and limited accuracy. The ability of EXAFS to determine the local structure around a specific atom is extremely useful in the study of multicomponent alloys and amorphous solids as well as dilute impurities and atoms on a surface. In multicomponent systems, the ability to study one component at a time greatly simplifies the analysis (*37, 38*). For dilute impurities or adsorbed species on a surface, the ability to isolate the absorption signal of the atom of interest by using fluorescence (*20*) or Auger (*39*) detection greatly enhances the sensitivity of the technique to the structure of interest.

EXAFS studies of highly disordered systems have suffered from the lack of a detailed understanding of the amplitude of the EXAFS signal. In addition, it is difficult to evaluate the implications of the absence of low-$k$ information on the radial distribution function determined from EXAFS data obtained in a limited range of values of $k$. Finally, there is some reason for concern (*40*) that the amplitude of the EXAFS signal may be dependent on the other inelastic excitation channels that are available. For example, the same atom measured in a metal or an insulator may have different EXAFS amplitudes. In highly disordered systems, which have a skewed radial distribution function, the absence of useful low-$k$ data will distort the radial distribution function determined from the data in such a way as to emphasize the sharper parts of the distribution over the more slowly varying parts.

While many investigators have commented on these difficulties, a study of the simple solids silver and zinc has clearly demonstrated their impact (*41*). The same study also showed that the linear polarization of the synchrotron beam could be used to obtain angular as well as radial information. By rotating the zinc crystal so that either the $c$ or the $a$ axis was parallel to the direction of x-ray polarization, it was possible to observe the shorter Zn-Zn distance along the $a$ direction or the 10 percent longer bond along the $c$ direction (*42*). So, in principle, for a single-crystal sample one can determine the geometry as well as the radial distribution function.

The problems described above have probably affected some of the quantitative determinations based on EXAFS studies of highly disordered systems, and may in fact limit the usefulness of the EXAFS technique for the study of these systems. However, interesting results are still obtainable.

Various other glassy, amorphous, and dilute-impurity systems have been studied by EXAFS (*43*). However, these are basically preliminary studies and will not be discussed in detail.

Like fluorescence detection of EXAFS, the Auger electron detection scheme has been very valuable in enhancing the sensitivity for dilute species (*39*). It has made it possible to measure the EXAFS spectrum of a single atomic layer on a crystal surface. As in fluorescence work, each atom is characterized by specific Auger energies. Thus, by setting the Auger electron detector at the energy of the desired species, one can determine the absorption spectrum by measuring the Auger intensity as a function of the energy of the incident photon beam. This procedure has been successfully implemented in a study of iodine atoms adsorbed on a silver [III] surface. At monolayer coverages (about $10^{13}$ atoms in the beam) the signal observed was sufficient to measure a usable spectrum in about 5 hours (*44*). In addition to determining the average I-Ag bond distance, it is possible to determine the position of the adsorbed atom with respect to the surface by measuring the spectrum with the polarization of the photon beam both perpendicular and parallel to the crystal surface. The development of this technique as a structural probe should be of great help in understanding surface phenomena.

Adsorbed molecules on graphite surfaces have also been studied by EXAFS (*45*). Transmission methods can be used since a large fraction of the atoms in the graphite samples used are on a "surface." Studies of $Br_2$ adsorbed on grafoil, a form of expanded graphite, have

revealed interesting structural changes as a function of surface coverage (*46*).

The application of EXAFS to solids and surfaces is probably at this time the least developed use of the technique. This is because of the difficulties mentioned above and the extensive array of other structural techniques that have been developed in solid state physics. However, indications are that a significant increase in research in these areas is beginning, probably because of a growing appreciation that EXAFS can make a unique addition to the array of standard structural tools used to study solids.

## Conclusions

The breadth and the potential of the EXAFS technique should be clearly apparent even from this short review. This is in spite of the fact that the first experiments with synchrotron radiation were completed in 1972. The breadth of this technique and the other unique uses of synchrotron radiation for photoemission, scattering studies, and microscopy have prompted the approval this year of $40 million in funding for dedicated synchrotron radiation sources in the United States. The growth in this country is matched by significant growth in England, France, Germany, Italy, Russia, and Japan. This growth promises more than an expansion of the existing capability. In newly designed storage rings dedicated to synchrotron radiation research (as opposed to high-energy physics) the brightness of the emitted synchrotron radiation is enhanced by factors of $10^3$ to $10^6$. Beams as intense as $10^{15}$ photons per second per electron volt or 1 watt per electron volt may be possible when wiggler devices are used (*47*); with such intense beams the technique might be extended to naturally occurring concentrations in living organisms—$10^{-5}$ to $10^{-6}$ molar. With the development of parallel detection schemes, measurements on more concentrated systems may be made in milliseconds; this would make it possible to follow a chemical reaction in real time.

The localization of resources and experimental capability at a few centralized institutions is, of course, a new experience for the chemical, biological, and solid state communities. However, if the psychological and sociological state of these sciences adapts as rapidly as the technology, the next decade should see a great increase in the structural information available to increase our understanding of physical, biological, and chemical phenomena.

### References and Notes


1. W. Kossel, *Z. Phys.* **1**, 119 (1920); R. de L. Kronig, *ibid.* **70**, 317 (1931); *ibid.* **75**, 191 (1932); *ibid.*, p. 468.
2. D. E. Sayers, F. W. Lytle, E. A. Stern, *Adv. X-Ray Anal.* **13**, 248 (1970); F. W. Lytle, D. E. Sayers, E. A. Stern, *Phys. Rev. B* **11**, 4825 (1975); E. A. Stern, D. E. Sayers, F. W. Lytle, *ibid.*, p. 4836.
3. H. Petersen, *Z. Phys.* **98**, 569 (1936).
4. A. I. Kostarev, *Zh. Eksp. Teor. Fiz.* **9**, 267 (1939).
5. L. Azaroff and D. Pease, *X-ray Spectroscopy* (McGraw-Hill, New York, 1974), chap. 5.
6. B. M. Kincaid and P. Eisenberger, *Phys. Rev. Lett.* **34**, 1361 (1975).
7. ———, D. Sayers, *Phys. Rev. B*, in press.
8. B. M. Kincaid, thesis, Stanford University (1974).
9. P. H. Citrin, P. Eisenberger, B. M. Kincaid, *Phys. Rev. Lett.* **36**, 1346 (1976); P. A. Lee, B. K. Teo, A. L. Simons, *J. Am. Chem. Soc.* **99**, 3856 (1977).
10. C. A. Ashley and S. Doniach, *Phys. Rev. B* **11**, 1279 (1975).
11. P. A. Lee and J. B. Pendry, *ibid.*, p. 2795.
12. P. A. Lee and G. Beni, *ibid.* **15**, 2862 (1977).
13. J. Reed, P. Eisenberger, B. K. Teo, B. M. Kincaid, *J. Am. Chem. Soc.* **99**, 5217 (1977); B. K. Teo, P. A. Lee, A. L. Simons, P. Eisenberger, B. M. Kincaid, *ibid.*, p. 3854.
14. B. M. Kincaid, P. Eisenberger, K. D. Hodgson, S. Doniach, *Proc. Natl. Acad. Sci. U.S.A.* **72**, 2340 (1975).
15. L. H. Jensen, *Annu. Rev. Biochem.* **43**, 461 (1974).
16. K. D. Watenbaugh, L. C. Sieker, J. R. Herriot, L. H. Jensen, *Acta Crystallogr. Sect. B* **29**, 143 (1973).
17. R. G. Shulman, P. Eisenberger, W. E. Blumberg, N. A. Stombaugh, *Proc. Natl. Acad. Sci. U.S.A.* **72**, 4003 (1975).
18. D. E. Sayers, E. A. Stern, J. R. Herriot, *J. Chem. Phys.* **64**, 427 (1976).
19. B. Bunker and E. A. Stern, *Biophys. J.* **19**, 253 (1977).
20. R. G. Shulman, P. Eisenberger, B. K. Teo, B. M. Kincaid, G. S. Brown, *J. Mol. Biol.*, in press; J. Jaklevic, J. A. Kirby, M. P. Klein, A. S. Robertson, G. Brown, P. Eisenberger, *Solid State Commun.* **23**, 679 (1977).
21. K. D. Watenbaugh, L. C. Sieker, L. H. Jensen, unpublished data.
22. M. F. Perutz, *Br. Med. Bull.* **32**, 193 (1976).
23. ———, *Nature (London)* **228**, 726 (1970); J. L. Hoard, *Science* **174**, 1295 (1971).
24. P. Eisenberger, R. G. Shulman, G. S. Brown, S. Ogawa, *Proc. Natl. Acad. Sci. U.S.A.* **73**, 491 (1976).
25. P. Eisenberger, R. G. Shulman, B. M. Kincaid, G. S. Brown, S. Ogawa, *Nature (London)*, in press.
26. J. L. Hoard, in *Porphyrins and Metallo-porphyrins*, K. M. Smith, Ed. (Elsevier, Amsterdam, 1975), p. 317.
27. S. P. Cramer, W. Gillum, R. O. Hodgson, L. E. Mortensen, *SSRP (Stanford Synchrotron Radiation Project) 4th Annu. Users Meet. Rep.* (1977), p. 63.
28. B. K. Teo, P. Eisenberger, J. Reed, J. K. Baston, S. J. Lippard, *J. Am. Chem. Soc.*, in press.
29. F. W. Lytle, D. E. Sayers, E. B. Moore, Jr., *Appl. Phys. Lett.* **24** (No. 2), 45 (1974).
30. J. Reed, P. Eisenberger, B. K. Teo, B. M. Kincaid, *J. Am. Chem. Soc.* **100**, 2375 (1978).
31. J. Reed and P. Eisenberger, *Acta Crystallogr.*, in press.
32. P. B. Hitchcock, M. McPartlin, R. Mason, *Chem. Commun.* (1969), p. 3671.
33. P. Eisenberger and B. M. Kincaid, *Chem. Phys. Lett.* **36**, 134 (1977).
34. A. Fontaine, P. Lagarde, D. Raoux, M. P. Fontana, G. Maisano, P. Migilardo, F. Wanderlingh, in preparation.
35. D. R. Sandstrom, H. W. Dodgen, F. W. Lytle, *J. Chem. Phys.* **67**, 473 (1977).
36. B. K. Teo, P. Eisenberger, B. M. Kincaid, *J. Am. Chem. Soc.* **100**, 3225 (1978).
37. D. E. Sayers, F. W. Lytle, E. A. Stern, *Amorphous and Liquid Semiconductors* (North-Holland, Amsterdam, 1974), p. 403.
38. T. M. Hayes, P. N. Sen, S. H. Hunter, *J. Phys. C* **9**, 4357 (1976); T. M. Hayes and S. H. Hunter, in *The Structure of Noncrystalline Materials*, P. H. Gaskell, Ed. (Taylor & Francis, London, 1977), p. 69.
39. P. A. Lee, *Phys. Rev. B* **13**, 5261 (1976).
40. J. J. Rehr, E. A. Stern, R. L. Martin, E. R. Davidson, *ibid.*, in press.
41. P. Eisenberger and G. Brown, in preparation.
42. G. S. Brown and P. Eisenberger, *Solid State Commun.* **24**, 201 (1977).
43. S. H. Hunter, A. Bienenstock, T. M. Hayes, in *The Structure of Noncrystalline Materials*, P. H. Gaskell, Ed. (Taylor & Francis, London, 1977), p. 73; D. E. Sayers, E. A. Stern, F. W. Lytle, *Phys. Rev. Lett.* **35**, 589 (1975); J. B. Boyce, T. M. Hayes, W. Stutius, J. C. Mikkelsen, Jr., *ibid.* **38**, 1313 (1977).
44. P. H. Citrin, P. Eisenberger, R. Hewitt, *Phys. Rev. Lett.*, in press.
45. E. A. Stern, *J. Vac. Sci. Technol.* **14**, 461 (1977).
46. ———, D. E. Sayers, J. G. Dash, H. Shechter, B. Bunker, *Phys. Rev. Lett.* **38**, 767 (1977).
47. B. M. Kincaid, *J. Appl. Phys.* **48**, 2684 (1977).